Published in : Journal of Power Sources (2023), vol. 55, 232410
DOI: doi:10.1016/j.jpowsour.2022.232410
Status : Postprint (Author's version)

FROM Na_2FePO_4F/CNT TO $NaKFePO_4F$/CNT AS ADVANCED CATHODE MATERIAL FOR K-ION BATTERIES

Jérôme Bodart [a], Nicolas Eshraghi [a b], Moulay Tahar Sougrati [c d], Frédéric Boschini [a], Pierre-Emmanuel Lippens [c d], Bénédicte Vertruyen [a], Abdelfattah Mahmoud [a]

[a] *GREENMAT, CESAM Research Unit, Department of Chemistry, University of Liège, Liège, 4000, Belgium*
[b] *Center for Low-Emission Transport, Battery Technologies, AIT Austrian Institute of Technology GmbH, Giefinggasse 2, 1210, Vienna, Austria*
[c] *Institut Charles Gerhardt Montpellier, UMR 5253 CNRS-UM-ENSCM, 1919, route de Mende, 34293 cedex 5, Montpellier, France*
[d] *RS2E, CNRS, Amiens, France*

KEYWORDS: Phosphate-based cathode; Spray-drying; K-ion batteries; Na-ion batteries

ABSTRACT

The Na_2FePO_4F/CNT composite investigated in this work was prepared by an optimized and easily scalable spray-drying process, resulting in an excellent initial discharge specific capacity of 123 mAh/g at C/15 when cycled against sodium. This NFPF/CNT composite was able to intercalate potassium ions reversibly with a promising specific capacity of 80 mAh/g after optimization of the electrolyte composition. Electrochemical desodiation was the key factor to reach outstanding performance as a cathode material in K-ion batteries, with the $NaKFePO_4F$/CNT composite leading to a stable capacity of 114 mAh/g at C/15 rate (99% of the theoretical capacity), one of the highest capacity values reported for K-ion technology.

HIGHLIGHTS

- $NaKFePO_4F$/C is prepared by electrochemical ion exchange.
- Na_2FePO_4F/C is evaluated as novel K-ion batteries cathode.
- Comparison of electrochemical performance of Na_2FePO_4F/C in SIB and KIB.
- $NaKFePO_4F$/C exhibits excellent electrochemical performance in KIB.

Published in : Journal of Power Sources (2023), vol. 55, 232410
DOI: doi:10.1016/j.jpowsour.2022.232410
Status : Postprint (Author's version)

GRAPHICAL ABSTRACT

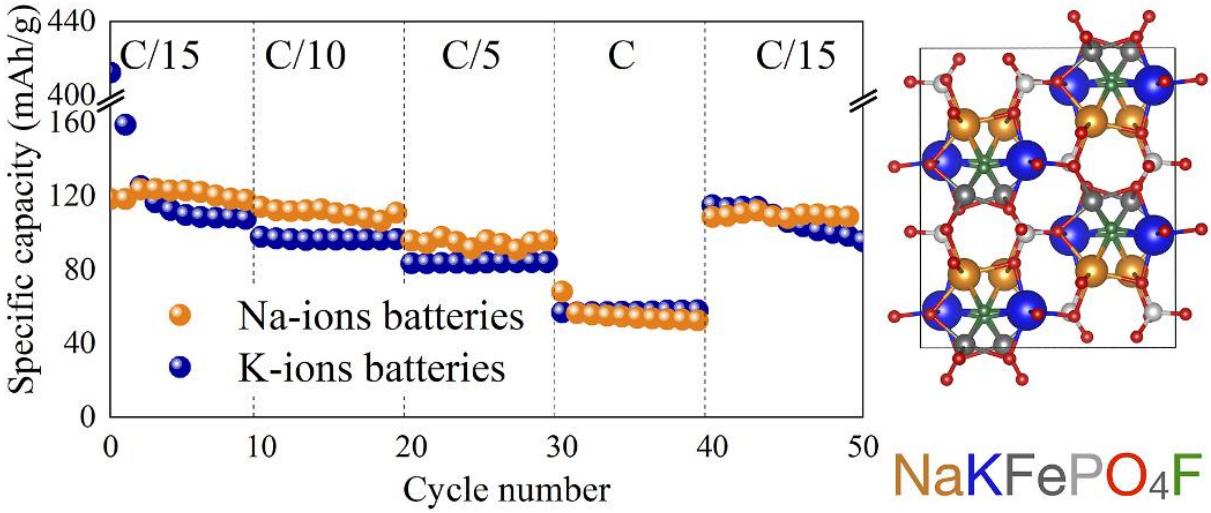

Na_2FePO_4F/CNT composite made by spray-drying process is developed for both Na-ion and K-ion batteries delivering a capacity of 124 mAh/g vs. Na and 114 mAh/g vs. K.

1. Introduction

The ongoing environmental transition will rely on a panel of energy storage technologies, including electrochemical storage. Next to Li-ion batteries (LIBs) [1], alternatives based on elements more abundant than lithium are needed. The development of Na-ion batteries (SIBs) has received huge interest over the past decade [2] and K-ion batteries (KIBs) have recently emerged as a fast-growing research topic [2-4]. KIBs share with SIBs the advantage of relying on an alkaline element that is very abundant, well-distributed geographically, and cheaper than lithium [3-5]. In addition, potassium offers a reduction potential close to that of lithium, so KIBs should reach a higher energy density than SIBs, assuming an equivalent specific capacity. Another difference between SIBs and KIBs is that potassium inserts reversibly and efficiently into graphite [3,6], the standard anode material developed for LIBs.

In both cases (SIBs and KIBs), polyanionic electrode materials [7,8] have been investigated as promising compounds, following the success story of $LiFePO_4$ for LIBs. Amongst polyanionic cathode materials for SIBs, the iron-based fluorophosphate Na_2FePO_4F (NFPF), first reported by Ellis et al. [9], offers a structure with 2D Na^+ pathways and low volume change on cycling. The relatively high theoretical capacity of 124 mAh/g [10,11] is combined with an operating voltage (3 V vs. Na^+/Na) boosted by the presence of fluorine to reach a theoretical energy density of 375 Wh/kg [10,12]. This favorable set of properties is the driving force behind the sustained interest in NFPF, exemplified by the publications in Table 1. As can be seen in this table, various synthesis processes and strategies have been explored to compensate for the relatively poor intrinsic electronic conductivity typical of (fluoro)-phosphates [10,12] and enhance the electrochemical performance of NFPF in SIBs. The synthesis processes include the solid-state route [10-17], hydrothermal/solvothermal processes [18-21], sol-gel routes [22-25] and a few less common

Published in : Journal of Power Sources (2023), vol. 55, 232410
DOI: doi:10.1016/j.jpowsour.2022.232410
Status : Postprint (Author's version)

procedures such as soft templating [26], electrospinning [27] or ultrasonic spray pyrolysis [28]. Strategies to improve electronic conductivity mostly rely on particle size reduction [13,19,26,27] and one-pot [10,18,23] or post-synthesis [14,15,19] carbon coating/encapsulation.

Table 1. *A non-exhaustive list of synthesis processes and strategies to enhance the electrochemical performance of NFPF as cathode material for Na-ion batteries.*

Synthesis Process	**Reported discharge capacity**	**Strategy to enhance the electrochemical performance**	**Reference**
Solid-state	110 mAh/g at C/20	Carbon coating with ascorbic acid	[10]
Solid-state	108.6 mAh/g at C/10	Nanosizing with polyfurfuryl alcohol as size reducing agent + carbon coating from glucose reduction	[11]
Solid-state	100-110 mAh/g at C/10	Coating with ascorbic acid and partial substitution of iron by Mn	[12]
Multistep solid-state	110 mAh/g at C/10	Polyol coating + Nanosizing	[13]
Multistep solid-state	123.1 mAh/g at C/5	Coating with conductive polymer PEDOT	[14]
Multistep solid-state	115 mAh/g at C/10	Metal-organic framework and mesoporous carbon network	[15]
Ball milling combined with solid-state	114 mAh/g at C/10	Mesoporous composite	[16]
Solid-state	117 mAh/g at C/10	Green carbon coating with ascorbic acid	[17]
Solvothermal	114.3 mAh/g at C/10	Carbon coating with glucose	[18]
Hydrothermal	118 mAh/g at C/10	Nanoshaping into nanorod and carbon composite by ball mixing with CNT and GN	[19]
Solvothermal	120.1 mAh/g at C/10	Double-shelled hollow microsphere composite with carbon	[20]
Hydrothermal	80 mAh/g at C/10	Crystalline transformation to alpha-NFPF	[21]
Sol-gel	100 mAh/g at C/10	Carbon composite by reduction of citric acid or ascorbic acid or urea during	[22]

Published in : Journal of Power Sources (2023), vol. 55, 232410
DOI: doi:10.1016/j.jpowsour.2022.232410
Status : Postprint (Author's version)

		synthesis	
Sol-gel	114.3 mAh/g at C/10	Biocarbon nanocomposite hollow sphere from yeast cell	[23]
Ultra-rapid combustion	70 mAh/g at C/10	Carbon composite from citric acid	[24]
Sol-gel	115.5 mAh/g at C/10	Porous sponge-like morphology and composite with carbon from oxalic acid	[25]
Soft templating	116 mAh/g at C/10	Nanosizing by high-energy ball milling	[26]
Electrospinning	117.8 mAh/g at C/10	Nanosizing and composite structuration with carbon fibers	[27]
Ultrasonic spray pyrolysis	89 mAh/g at C/10	Carbon coating by sucrose reduction + hollow sphere structuration	[28]
Spray-drying assisted solid-state	**123.8 mAh/g at C/15**	**Carbon nanotubes network inside particles**	**This work**

A few years ago [29-31], our group investigated a synthesis route based on the spray-drying technique, to benefit from the well-known advantages of spray-drying in terms of repeatability and industrial up-scalability. Carbon nanotubes (CNT) were added to the aqueous solution of the NFPF precursors to ensure the formation of a NFPF/CNT composite after heat treatment in argon. At the time, the NFPF/CNT electrode performance was tested by cycling against lithium and the relatively large size of the composite particles limited the experimental specific capacity to about 80% of the theoretical capacity.

In the present work, we report an improved spray-drying procedure where the smaller particle size offered by bi-fluid nozzle atomization results in competitive performance of the NFPF/CNT material when cycled against sodium. This optimized material is then tested for the first time as a candidate cathode material in KIBs, first by cycling the as-obtained NFPF against sodium and then by cycling against potassium after a pre-charging step.

2. Experimental

NFPF/CNT powders were prepared by annealing in argon of an intermediate obtained by spray-drying. In a typical synthesis, 0.1 mol of iron powder (99.9%, abcr GmbH) is dissolved in a solution of 0.075 mol of citric acid (Alfa Aesar) in a mixture of 100 mL of milliQ water (18.2 MΩ/cm) and 0.2 mol of acetic acid by heating under reflux at 90 °C under argon. After 24 h, 0.1 mol of $NH_4H_2PO_4$ (Sigma Aldrich), 0.1 mol of NaF (Sigma Aldrich), 0.1 mol of NaOH (Sigma Aldrich), 15 wt% (with

Published in : Journal of Power Sources (2023), vol. 55, 232410
DOI: doi:10.1016/j.jpowsour.2022.232410
Status : Postprint (Author's version)

respect to NFPF) of carbon nanotubes (AQ30X suspension from Nanocyl) and 900 mL of milliQ water (18.2 MΩ/cm) are added to the solution, which is then homogenized by magnetic stirring under argon for 1 h at room temperature. This liquid feedstock is spray-dried in air using a Niro mobile minor spray dryer (inlet temperature: 160 °C; outlet temperature: 90 °C; bi-fluid injector with 25 mL/min feed rate and 3 bars of air pressure). The as-sprayed powder is then heated at 600 °C for 2 h under an Ar flow with a heating rate of 150 °C/h.

X-ray powder diffraction (XRD) data were collected using a Bruker D8 diffractometer (Cu K_α radiation; 10–60° 2θ range; 0.02° step size). The powder morphology was examined by scanning electron microscopy (XL30 FEG-ESEM, FEI) and by transmission electron microscopy (200 kV, TECNAI G2 TWIN, FEI). Nitrogen (N_2) adsorption-desorption isotherms were measured with a Micromeritics ASAP 2020 Plus system after degassing at 150 °C for 6 h.

^{57}Fe transmission Mössbauer spectra were recorded at room temperature in the ±12 mm/s velocity range with a constant-acceleration spectrometer and a ^{57}Co(Rh) source. The Mössbauer absorbers were prepared with 40 mg/cm^2 of NFPF/CNT mixed with boron nitride. The spectrometer was calibrated at room temperature with the magnetically split sextet spectrum of a high-purity α-Fe foil as the reference for isomer shifts. The spectral parameters isomer shift (δ), quadrupole splitting (ΔEq), linewidth (Γ), and relative resonance areas (A) of the different spectral components were determined with Lorentzian curves using the Fullham program. The validity of fits was judged based on minimizing the number of parameters and χ^2 values.

The standard electrochemical measurements were performed in CR2032 coin cell configuration. The positive electrode was prepared by mixing the active material, carbon black (CB), and polyvinylidene fluoride (PVDF) to reach a mass ratio NFPF:C_{total}:PVDF of 7:2:1. After mixing 600 mg of mixed powders in 3 mL N-methyl-2-pyrrolidone (NMP) with 5 mm zirconia balls in a 50 mL zirconia jar for 1 h (Retsch PM400/2 planetary mill, 150 RPM, alternate rotation mode), the slurry was tape cast on aluminum foil by the doctor blade method and then dried at 110 °C for 12 h under vacuum. The electrodes were then cut to obtain electrode discs of 15 mm in diameter with about 1 mg/cm^2 mass loading. The coin cells were assembled in an argon-filled glove box using a Whatman® filter separator. For Na half-cells, the electrolyte was 1 M $NaPF_6$ dissolved in propylene carbonate (PC) and sodium foil was used as the counter and reference electrode (Na half-cell). For K half-cells, several electrolytes were used: (i) 0.8 M KPF_6 in PC with 10 wt% of fluoroethylene carbonate (FEC), (ii) 0.8 M KPF_6 in ethylene carbonate (EC) and PC (1:1 v:v) and (iii) 0.8 M KPF_6 in EC:PC (1:1 v:v) with 10 wt% of FEC. Metallic potassium was used as the counter and reference electrode (K half-cell). Galvanostatic cycling tests were carried out using a Neware BTS4000 potentiostat in the voltage range of 2–4.2 V *vs.* Na^+/Na and K^+/K, except for few tests in Na half-cells in the range of 2–4.5 V, at different rates from C/15 to C where C is the theoretical current density for a complete charge or discharge. During precharging experiments to remove sodium from the pristine material, the NFPF/CNT material was first fully charged in a Na half-cell and maintained at the potential of 4.2 V for 1 h. The coin cell was opened, and the electrode was thoroughly washed with diethyl carbonate solvent and dried overnight. The K half-cell was then assembled following initial conditions with K metal as anode and 0.8 M KPF_6 in EC:PC (1:1 V:V) as the electrolyte, using a

Published in : Journal of Power Sources (2023), vol. 55, 232410
DOI: doi:10.1016/j.jpowsour.2022.232410
Status : Postprint (Author's version)

voltage range of 1.5–4.2 V *vs.* K^+/K. A VMP3 Bio-logic potentiostat was used to perform electrochemical impedance spectroscopy (EIS) with 5 mV amplitude in the frequency range from 1 MHz to 10 mHz and cyclic voltammetry between 1 and 5 V *vs.* Na^+/Na or K^+/K at a speed rate of 0.05–1 mV/s. The EIS data were fitted with the Aftermath software from Pine Research Instrumentation. All electrochemical tests were carried out at room temperature.

3. Results and discussion

3.1. COMPOSITION, STRUCTURE, AND MICROSTRUCTURE OF NFPF/CNT

The synthesis conditions described in the experimental section (dissolution of iron under argon, spray-drying in air, heat-treatment at 600 °C for 2 h in argon) were optimized during preliminary tests to prevent the formation of metallic iron by carbothermal reduction during the heat treatment.

Fig. 1 presents the main characteristics of the NFPF/CNT powder obtained with the optimized synthesis conditions. All peaks in the XRD pattern (Fig. 1a) are similar to those in the sample without CNT and can be indexed in the NFPF orthorhombic structure [9] with cell parameters a = 5.23 Å, b = 13.86 Å and c = 11.79 Å. The average crystallite size estimated with the Scherrer formula is about 27 nm, while the SEM images (Fig. 1b) show collapsed granules with diameters from 1.5 to 5 µm. This microstructure is in good agreement with our previous works on the addition of CNT in the spray-drying solution [29,32-34] and is attributed in the literature to the formation of a viscoelastic shell during the drying step [32,33]. The BET specific surface area is in the 100 m^2/g range, also due to the presence of carbon nanotubes. The absence of metallic iron or other iron-containing secondary phases in the XRD pattern is confirmed by the Mössbauer analysis presented in Fig. 1c and d. The experimental spectrum has an asymmetric shape that can be fitted by using two doublets (75 at% Fe) with average isomer shifts and quadrupole splitting typical of Fe(II) and one doublet (25 at% Fe) with parameters corresponding to Fe(III) in sodium-poor NFPF ($Na_{2-x}FePO_4F$) [35]. The presence of Fe(III) in the NFPF phase obtained by spray-drying was studied in detail by operando Mössbauer spectroscopy in a previous work [30] where it was found that a Fe(III)-free NFPF phase is recovered after one galvanostatic cycle in Li-ion batteries.

Published in : Journal of Power Sources (2023), vol. 55, 232410
DOI: doi:10.1016/j.jpowsour.2022.232410
Status : Postprint (Author's version)

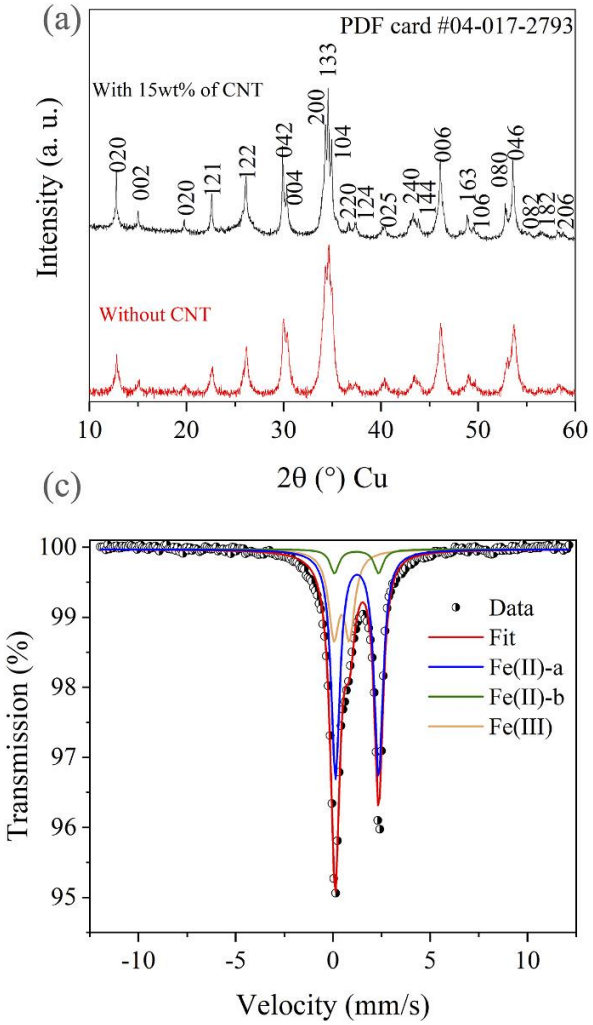

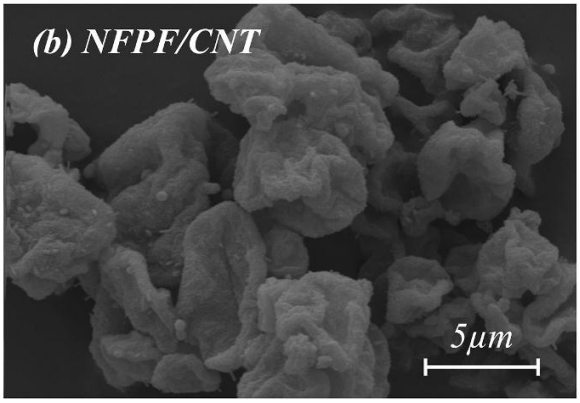

(d)	Fe(II)-a	Fe(II)-b	Fe(III)
δ (mm/s)	1.24(1)	1.21(2)	0.45(1)
ΔEq (mm/s)	2.22(1)	2.27(4)	0.80(1)
Γ (mm/s)	0.54(1)	0.54(1)	0.66(1)
Area (%)	65(1)	7(1)	28(1)

Figure 1. *NFPF/CNT powder after 2 h at 600 °C in argon : (a) X-ray diffractogram indexed in the Pbcn space group and comparison with the sample without CNT, (b) secondary electron micrograph, (c) ^{57}Fe Mössbauer spectrum, and (d) corresponding hyperfine parameters obtained with a 3-doublet fit.*

Fig. 2 shows further details of the distribution of carbon nanotubes in the inorganic matrix; the higher magnification SEM micrograph (Fig. 2b) shows the carbon nanotubes within and at the surface of the NFPF matrix, while the inter-particle connection is confirmed by the transmission electron micrograph in Fig. 2c. EDX mapping in the SEM did not reveal any anomaly in the homogeneity of the Na, Fe, P, and F elemental distribution (see Fig. S1 in Supplementary Information).

Published in : Journal of Power Sources (2023), vol. 55, 232410
DOI: doi:10.1016/j.jpowsour.2022.232410
Status : Postprint (Author's version)

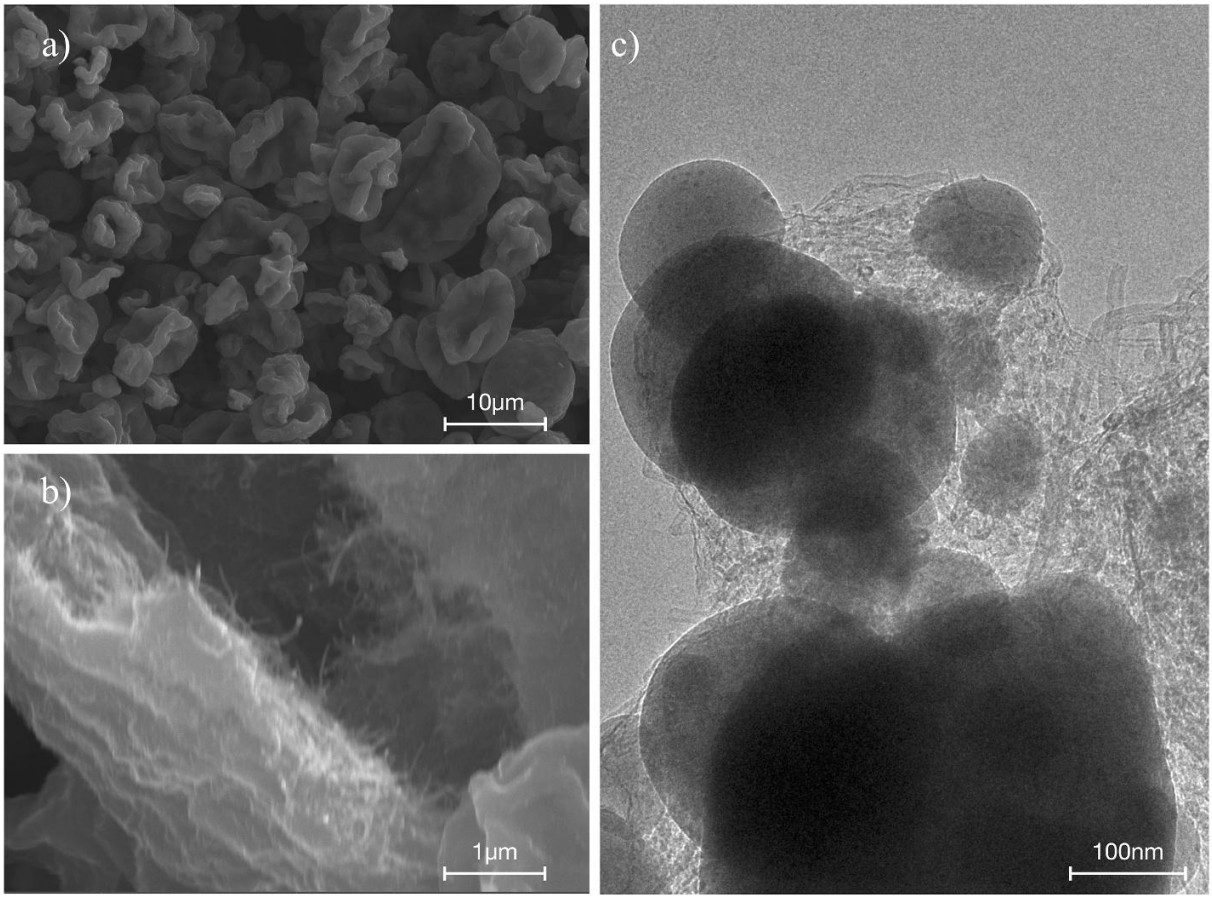

Fig. 2. (a, b) Secondary electron micrographs and (c) transmission electron micrograph of NFPF/CNT powder after 2 h at 600 °C in argon.

3.2. NFPF/CNT CYCLED AGAINST SODIUM

The NFPF/CNT powder was first characterized in Na half-cells to assess its performance and validate its potential to be used in SIB using the easily upscalable spray-drying synthesis method. Fig. 3 shows the galvanostatic cycling tests performed in the voltage window of 2–4.2 V *vs*. Na^+/Na. The evolution of the discharge capacity as a function of the cycling rate is presented in Fig. 3a and the associated charge-discharge profiles are illustrated in Fig. 3b. The highest discharge specific capacity (123 mAh/g) is obtained at C/15 and corresponds to 99% of the theoretical capacity. Average discharge capacities of 121.6, 113.5, 94.7, and 55.7 mAh/g are obtained at C/15, C/10, C/5, and 1C cycling rates, respectively, with a coulombic efficiency of more than 98.5% at all cycling rates. Returning to C/15 after the rate capability test, the electrode is still able to deliver a discharge capacity of 110 mAh/g. The charge-discharge profiles in Fig. 3b suggest the presence of two distinct discharge plateaus at C/15 and C/10 around 2.75 and 3 V. The cycling test for 50 cycles at C/15 in Fig. 3c shows a maximum discharge capacity of 123 mAh/g and 95% of capacity retention. When cycling at C/5 (Fig. 3d) the maximum capacity is 104 mAh/g and 90% of capacity is retained after 100 cycles.

Published in : Journal of Power Sources (2023), vol. 55, 232410
DOI: doi:10.1016/j.jpowsour.2022.232410
Status : Postprint (Author's version)

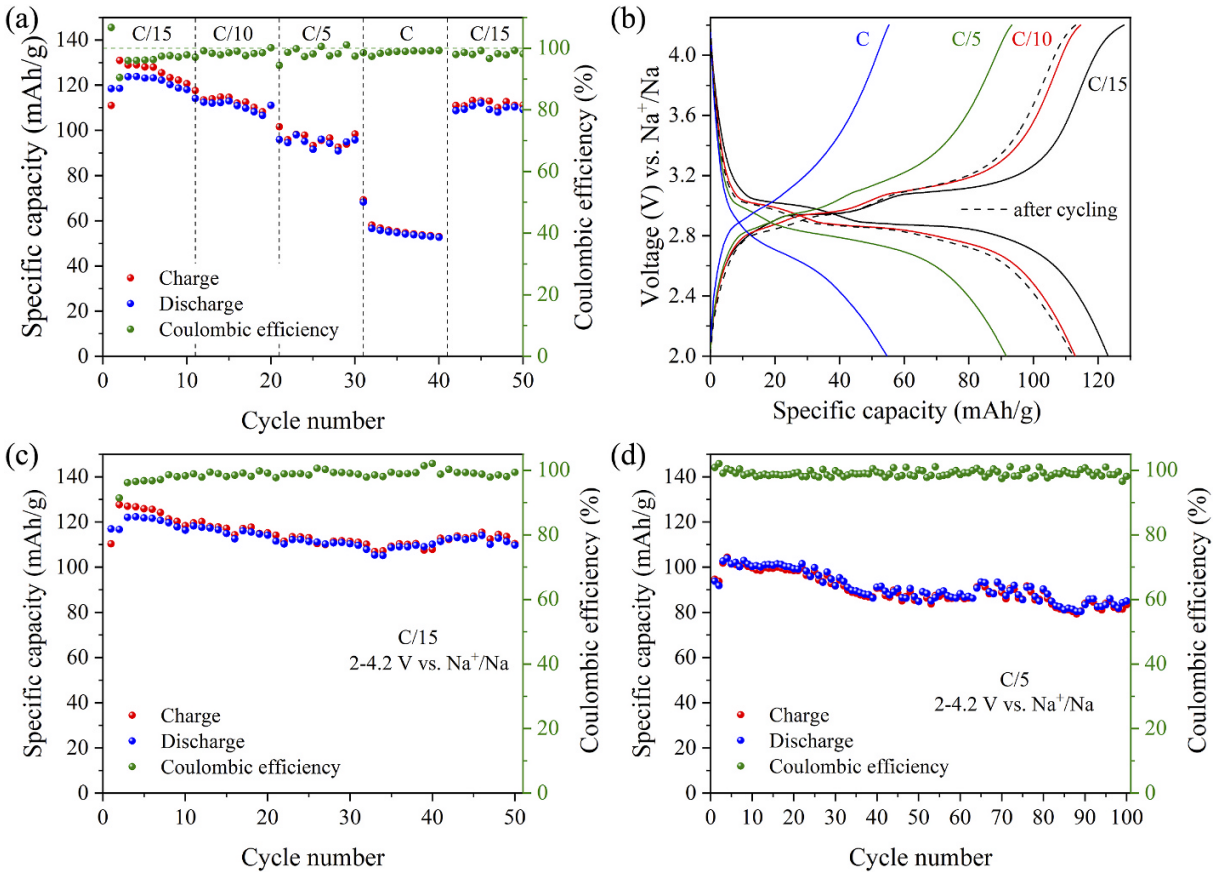

Figure 3. *NFPF/CNT in Na-half cell (room temperature) : (a) Specific capacity and coulombic efficiency vs. cycle number at C/15, C/10, C/5, and 1C rates in the voltage window 2–4.2 V vs. Na^+/Na. (b) Charge/discharge curves at C/15, C/10, C/5, and 1C rates from rate capability test. (c-d) Evolution of specific capacity and coulombic efficiency vs. cycle number at C/15 and C/5 rates. The fluctuations are associated with variations of the temperature during the cycling tests.*

Since Deng et al. reported that extra capacities could be obtained by partially removing the second Na from the NFPF structure [17], we performed some tests in the voltage range of 2.2–4.5 V *vs.* Na^+/Na (see Fig. S2 in Supplementary Information). However, this broadening of the voltage window did not notably increase the specific capacity values but markedly deteriorated the coulombic efficiency, which dropped to about 90% due to the degradation of the electrolyte at high voltage. Similarly, grinding did not improve electrochemical performance (Fig. S2), confirming that the well-distributed carbon network inside and at the surface of the NFPF particles is sufficient to ensure electronic conductivity.

As a complement to the galvanostatic cycling experiments, electrochemical impedance spectroscopy (EIS) was used to further characterize the properties of NFPF/CNT in a Na half-cell. The EIS spectra of NFPF and NFPF/CNT have similar shapes but show a strong decrease in the charge transfer resistance from 234 to 64 Ω due to the addition of CNT (Fig. S3), confirming the good electronic conductivity of the NFPF/CNT composite.

Published in : Journal of Power Sources (2023), vol. 55, 232410
DOI: doi:10.1016/j.jpowsour.2022.232410
Status : Postprint (Author's version)

3.3. NFPF/CNT CYCLED AGAINST POTASSIUM

Fig. 4 presents preliminary cycling tests that were performed on K half-cells in order to assess whether the NFPF phase is able to act as a cathode material for KIBs. Fig. 4a illustrates the rate performance at different current densities for NFPF/CNT in K half-cells in the voltage window of 2–4.2 V. Three different electrolyte compositions were evaluated: (i) 0.8 M KPF_6 in PC with 10 wt% of FEC (PC-FEC), (ii) 0.8 M KPF_6 in EC:PC (1:1 v:v) (EC-PC) and (iii) 0.8 M KPF_6 in EC:PC (1:1 v:v) with 10 wt% of FEC (EC-PC-FEC).

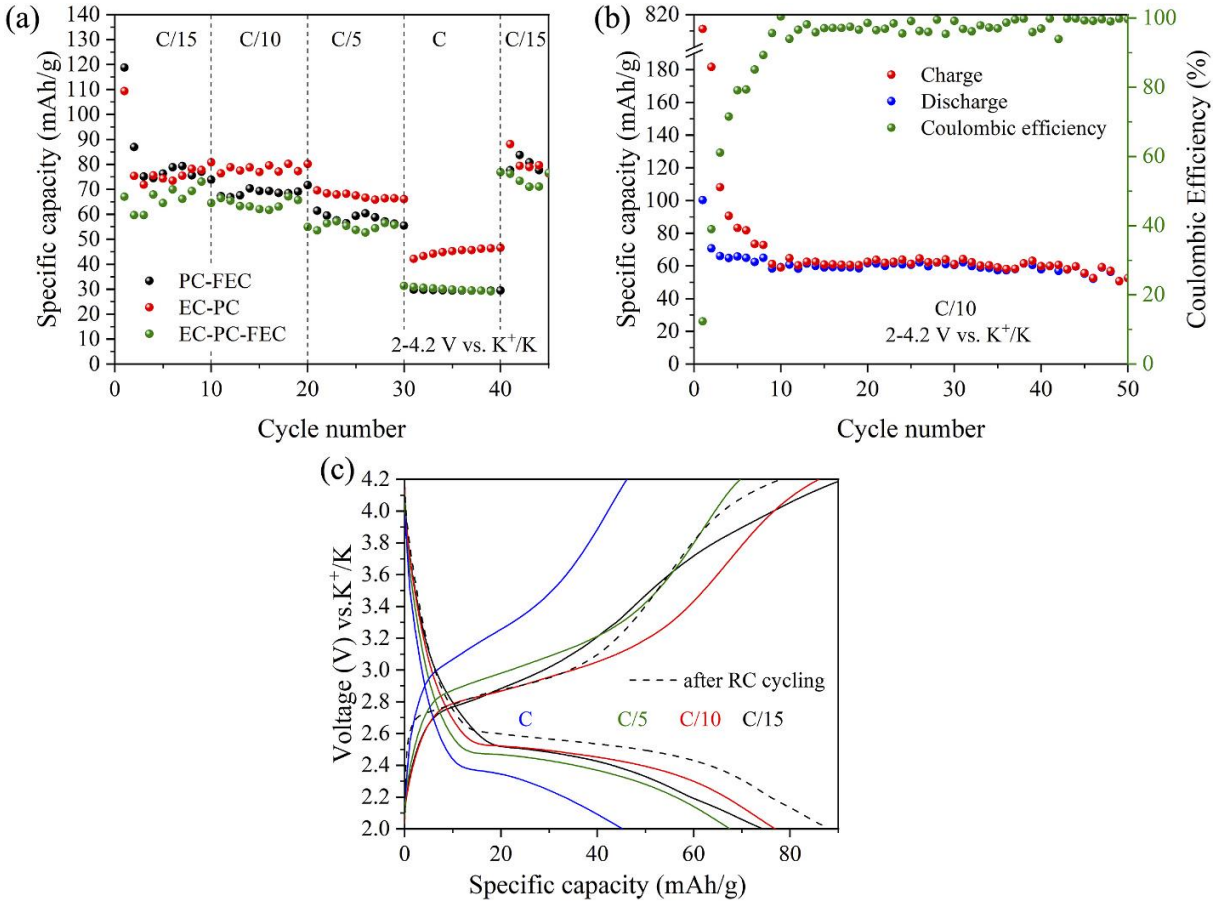

Fig. 4. *NFPF/CNT in K-half cell (room temperature) : (a) Evolution of discharge capacity vs. cycle number at C/15, C/10, C/5, and C rates, with different electrolytes: 0.8 M KPF_6 in PC with 10 wt% of FEC (black circles), 0.8 M KPF_6 in EC and PC (1:1) (red circles), and 0.8 M KPF_6 in EC and PC (1:1) with 10 wt% of FEC (green circles). (b) Evolution of discharge capacity vs. cycle number over 50 cycles at C/10 (red circles), with 0.8 M KPF_6 in EC and PC (1:1). (c) Charge/discharge curves extracted from the rate capability experiment at C/15, C/10, C/5, and 1C rates using 0.8 M KPF_6 in EC and PC.*

The first cycles at C/15 show that the PC-FEC and EC-PC electrolytes lead to a strong decrease of the specific capacity from 120 to 75 mAh/g, suggesting a secondary reaction. In the case of the EC-PC-FEC electrolyte, the capacity is about 70 mAh/g from the beginning. Using the additive-free 0.8 M KPF_6 in EC:PC electrolyte leads to higher capacity retentions during further cycles in the rate capability tests. The cells using this electrolyte exhibit discharge capacities of 75, 82, 68, 45, and 80

Published in : Journal of Power Sources (2023), vol. 55, 232410
DOI: doi:10.1016/j.jpowsour.2022.232410
Status : Postprint (Author's version)

mAh/g at C/15, C/10, C/5, 1C, and C/15 after high C-rate measurements, respectively (red circles in Fig. 4a). This represents 71% of the theoretical capacity of $NaKFePO_4F$ (115 mAh/g). The lower capacity observed at higher cycling rates is expected for such materials and is associated with kinetic limitations. The specific capacity of 79 mAh/g (69% of theoretical capacity) observed after the rate capability testing suggests stable structure and insertion properties of the material after going through a kinetically limiting cycling procedure. The obtained capacity with the other two electrolytes is similar except at the highest rate (1C), where the capacity obtained with the EC-PC electrolyte is almost two times higher than with the others. A cycling test was performed at C/10 rate for 50 cycles (Fig. 4b). After a strong irreversibility in the first cycle, the observed reversible capacity is about 70 mAh/g for the second cycle, decreases slightly over the next 10 cycles and stabilizes at 60 mAh/g, with a good coulombic efficiency. Fig. 4c shows the charge and discharge curves obtained at different C-rates; only one plateau can be observed at each cycling rate and the potentials *vs.* K^+/K are lower than *vs.* Na^+/Na, especially when taking into account the 0.22 V difference between Na^+/Na (−2.71 V *vs*. SHE) and K^+/K (−2.93 V *vs*. SHE).

In order to investigate this phenomenon, cyclic voltammograms were collected with 3-electrode Swagelok cells with sodium or potassium as negative and reference electrodes. As shown in Fig. 5, the peaks of the first charge (desodiation in both cases) were shifted by 0.24–0.26 V, close to the 0.22 V difference between Na^+/Na (−2.71 V *vs*. SHE) and K^+/K (−2.93 V *vs*. SHE). In the case of cycling against sodium, the first and second cycles displayed very little difference. On the contrary, the replacement of Na^+ ions by K^+ ions during cycling against potassium led to a shift of the peak potentials towards lower values. Indeed, the material being cycled is no longer Na_2FePO_4F but $NaKFePO_4F$. A similar decrease in potential when inserting/extracting K^+ ions was observed for $Na_3V_2PO_4F_3$ by Lin et *al*. [36], who related this phenomenon to the structure adaptations when larger K^+ ions replace Na^+ ions.

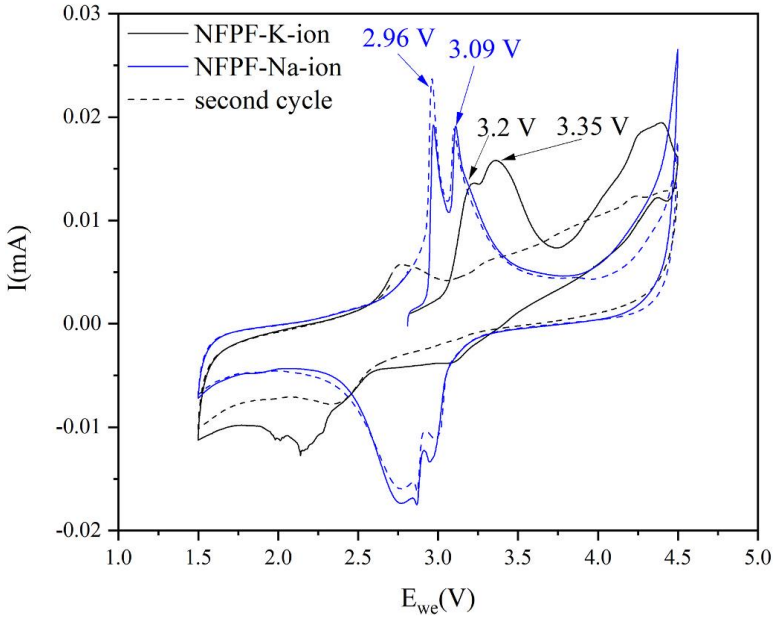

Fig. 5. Cyclic voltammetry test of NFPF/CNT in 3-electrode Swagelok cells with Na (in blue) or K (in black) as reference and counter electrodes (at 0.05 mV/s). The dotted lines represent the second cycles.

Published in : Journal of Power Sources (2023), vol. 55, 232410
DOI: doi:10.1016/j.jpowsour.2022.232410
Status : Postprint (Author's version)

3.4. NFPF/CNT CYCLED AGAINST POTASSIUM AFTER PRE-CHARGING

To enhance the electrochemical performance of NFPF/CNT as cathode material for KIBs, NFPF/CNT electrodes were first fully charged in Na half-cells to ensure the removal of one Na ion following the protocol described in the experimental section. These precharged electrodes were then tested in K half-cells, using 0.8 M KPF_6 in EC:PC (1:1 v:v) as electrolyte. Fig. 6 shows the results for three cells, in order to estimate the reproducibility of the observed behavior. After the first few cycles suffering from irreversibility (probably enhanced due to the transfer of the electrode from the Na half-cell to the K half-cell), the specific capacity stabilizes at higher values than in the non-pre-charged cells, with 114, 104, 88, 60, and 105 mAh/g at C/15, C/10, C/5, 1C, and back to C/15, respectively. The formation cycle to prepare $NaFePO_4F$ electrochemically allows to reach over 99% of the theoretical capacity at C/15. However, the charge/discharge profiles in Fig. 6b reveal the presence of an additional plateau at 3 V in the first charge (C/15), suggesting that Na^+ ions are still extracted during the first cycle in K half-cell. After a few cycles, only one plateau is visible. A similar behavior was observed by Lin et al., in 2019 when replacing progressively the Na^+ ions by K^+ ions in $Na_3V_2(PO_4)_2F_3$ [36]. These authors obtained a decent capacity of 100 mAh/g at 3.4 V, positioning this work among the best performing ones reported for a KIB cathode. The reversible capacity of 114 mAh/g at 3 V obtained here starting from NFPF confirms the huge interest to use Na^+ or Li^+ analog materials for the development of high capacity cathode materials for KIBs [36], in line with previous success of this strategy in the LIB-SIB context (delithiation by electrochemical charging followed by sodiation through discharging in sodium half-cell) [[37], [38], [39], [40]].

Published in : Journal of Power Sources (2023), vol. 55, 232410
DOI: doi:10.1016/j.jpowsour.2022.232410
Status : Postprint (Author's version)

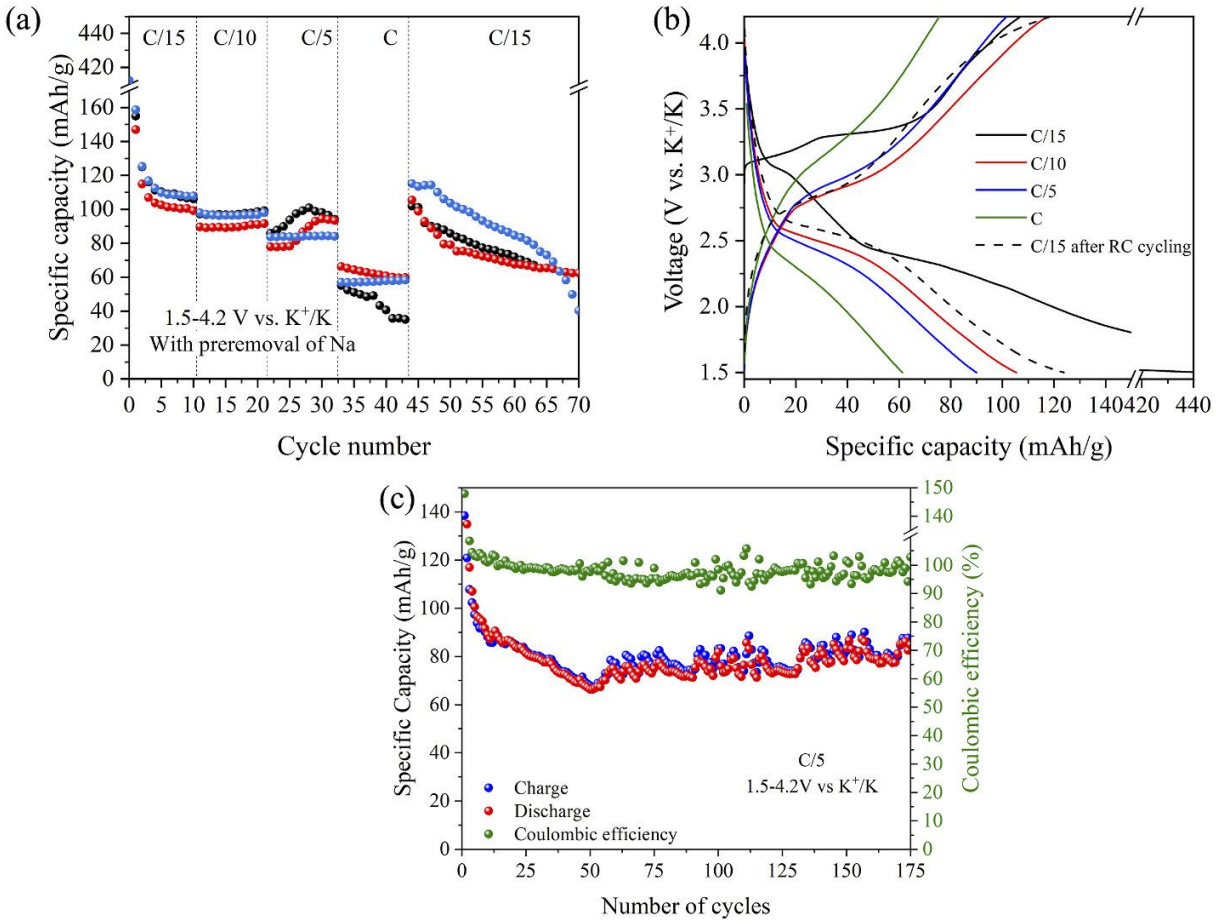

Fig. 6. *Pre-charged NFPF/CNT in K-half cell (room temperature) : (a) Evolution of discharge capacity vs. cycle number for 3 similarly-prepared electrodes with 0.8 M KPF_6 in EC:PC (1:1) as electrolyte and at C/15, C/10, C/5, 1C rates. (b) Charge/discharge curves extracted from the rate capability test of precharged NFPF/CNT in K half-cells at C/15, C/10, C/5, and 1C rates. (c) Evolution of discharge capacity vs. cycle number over 175 cycles at C/5. The oscillations after 50 cycles are due to central-heating-related temperature variations in the room.*

Fig. 6c shows long-term cycling against potassium at C/5. Over the first ten cycles, the already observed irreversibility led to a fading of the capacity to ~90 mAh/g. The variations during further cycles mostly reflect the variations in the temperature of the room. When discounting these oscillations, the capacity was rather stable (94% capacity retention from the 10th cycle to the 175th cycle) with an average coulombic efficiency of 98.5%.

The comparison between the behavior when cycling *vs*. Na and *vs*. K was further studied by cyclic voltammetry (CV). Fig. 7a presents the cyclic voltammograms *vs*. Na for scan rates between 0.05 mV/s and 1 mV/s. In agreement with the two-step mechanism $Na_2FePO_4F \rightarrow Na_{1.5}FePO_4F \rightarrow Na_1FePO_4F$ proposed by some authors [10,12], two oxidation peaks (A: 3 V, B: 3.2 V) and two reduction peaks (C: 2.75 V and D: 3 V) are observed at all scan rates. The maximum current of the redox peaks is plotted in Fig. 7b versus the square root of the scan rate. The observed linearity for both the oxidation and reduction peaks indicates that the diffusion process is limited by the diffusion of the sodium ions in the electrode material [[41], [42], [43]].

Published in : Journal of Power Sources (2023), vol. 55, 232410
DOI: doi:10.1016/j.jpowsour.2022.232410
Status : Postprint (Author's version)

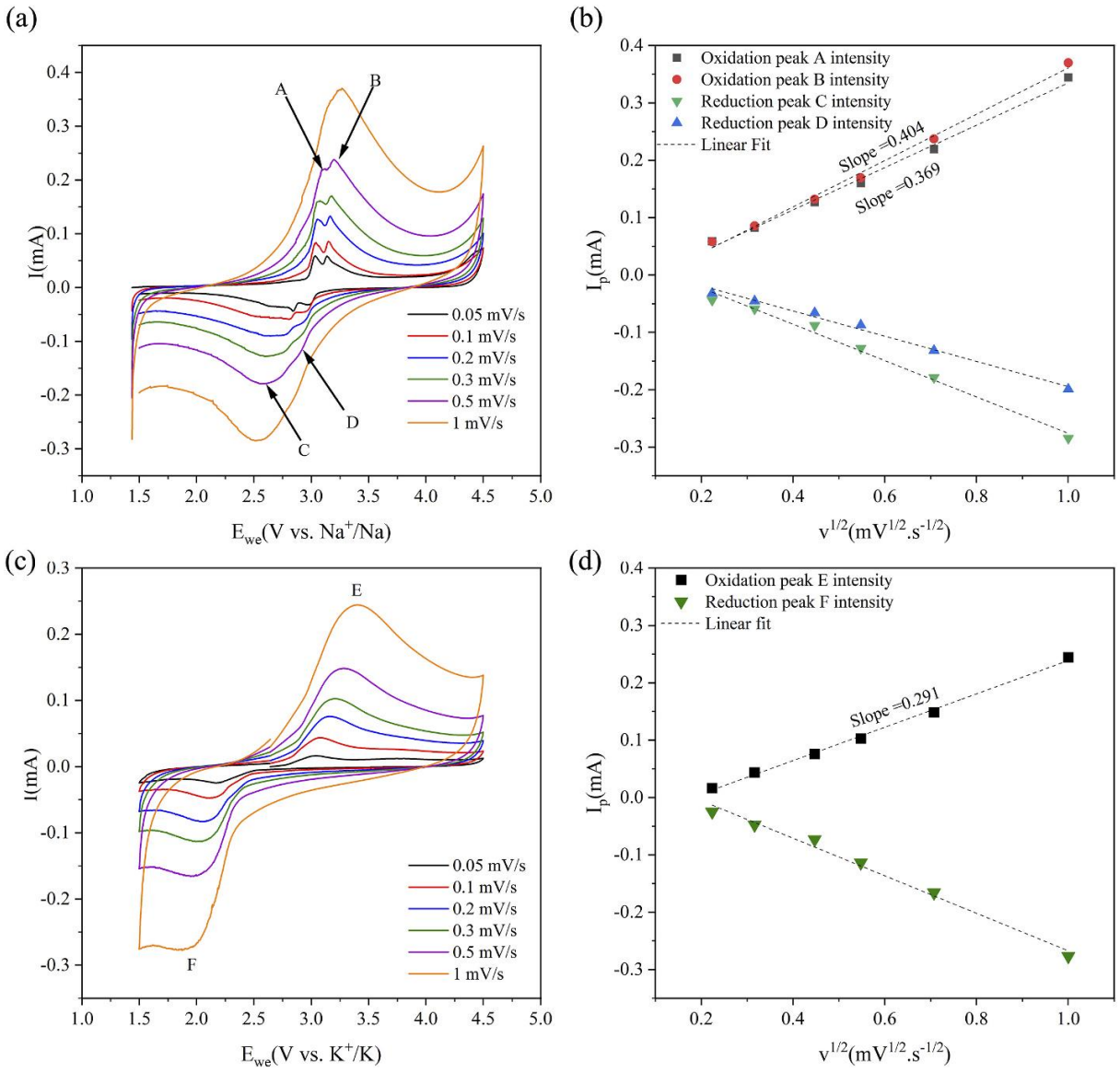

Fig. 7. (a,b) Cyclic voltammograms at scan rates between 0.05 and 1 mV/s and evolution of the peak current versus the square root of the scan rate for NFPF/CNT in Na-half cell. (c,d) Cyclic voltammograms at scan rates between 0.05 and 1 mV/s and evolution of the peak current versus the square root of the scan rate in K-ion half-cell after a precharge in Na-half cell.

Fig. 7c presents the results of a similar CV experiment performed *vs.* K with a pre-charged electrode. By comparison with the corresponding results against Na, only one oxidation peak and one reduction peak can be observed. There is also a displacement of the voltage peak depending on the scan rate: at 0.05 mV/s the oxidation peak (E) appears at 3.04 V, and at a higher scan rate (1 mV/s) the oxidation peak shifts to 3.40 V. The same phenomenon is observed for the reduction peak (F) shifting from 2.16 V at 0.05 mV/s to 1.89 V at 1 mV/s. Fig. 7d shows that the maximum current linearly depends on the square root of the scan rate. This linearity indicates that the diffusion process is limited by the potassium ion movement in the electrode material.

This linear relationship observed for both Na^+ and K^+ is described by the Randles- Ševčík equation (Eq. (1)) [41-43]: $I_p = 2.69\ 10^5\ n^{3/2}\ S\ (D_{A+})^{1/2}\ C_{A+}\ v^{1/2}$ (Eq. 1) Where I_p is the peak intensity current, n is the

Published in : Journal of Power Sources (2023), vol. 55, 232410
DOI: doi:10.1016/j.jpowsour.2022.232410
Status : Postprint (Author's version)

number of electrons, S is the effective surface area, D_{A+} is the diffusion coefficient of sodium/potassium ions and C_{A+} is the concentration of mobile A^+ ions (either Na^+ or K^+) in the electrode. The slope for the evolution of the oxidation peaks is 0.29 A $s^{1/2}$ $V^{-1/2}$ for the K half-cell and 0.37–0.40 mA $s^{1/2}$ $mV^{-1/2}$ for the Na half-cell, revealing a difference between the two experiments. In order to determine explicit values for the diffusion coefficients, it is necessary to make assumptions about the values of some of the parameters in the Randles-Sevcik equation, such as the effective surface area S. The detailed discussion provided in Supplementary Information (Table S1) first determines the diffusion coefficients using specific surface area (without CNT = 1.75 m^2/g) that is underestimated and then uses literature values of ~10^{-12} cm^2/s for D_{Na+} in Na_2FePO_4F [16,21,44] to arrive at a value of ~0.5 10^{-12} cm^2/s for D_{K+}. This slightly more difficult diffusion of the K^+-ions in the NFPF structure can be related to the fact that the ionic radius of K^+ is 1.33 Å where the Na^+-radius is only 0.97 Å [3]. The low decrease of the diffusion coefficient proves the electrochemical activity and potential applications of the NFPF phase as a cathode material for KIBs.

Conclusions

For the first time, cycling versus potassium was performed to investigate the electrochemical performance of NFPF/CNT. A discharge capacity of 80 mAh/g is obtained, which represents 71% of the theoretical capacity of $NaKFePO_4F$ with 0.8 M KPF_6 in EC:PC as the best amongst the tested electrolyte. The initial cycles present irreversibility that can be associated with the replacement of sodium by potassium in the crystal lattice. The pre-cycling of the material in a Na half-cell to remove Na before cycling in K half-cells led to improved performance with a specific capacity of 114 mAh/g at C/15, i.e., 99% of the theoretical capacity. These results highlight the potential of NFPF/CNT prepared by spray-drying as a cathode material for both SIBs and KIBs. *In situ* experiments will be needed to investigate the reaction mechanisms when cycling against K, while additional work on the effect of the electrolyte could help to reduce the irreversibility observed in the first cycles and increase the coulombic efficiency. The rate capability might be further enhanced by replacing part of the CNT with reduced graphene oxide, as in our previous work on $K_3V(PO_4)_2$ [34]. Other strategies would be down-sizing by grinding (without structure degradation) or tuning the spray-drying parameters to create smaller particles and adapting the heat treatment to suppress the carbothermal reduction.

CRediT authorship contribution statement

Jérôme Bodart: Conceptualization, Investigation, Formal analysis, Investigation, Writing – original draft, Writing – review & editing, Visualization. **Nicolas Eshraghi:** Validation, Formal analysis, Writing – review & editing. **Moulay Tahar Sougrati:** Validation, Formal analysis, Writing – review & editing. **Frédéric Boschini:** Project administration, Supervision, Funding acquisition. **Pierre-Emmanuel Lippens:** Validation, Formal analysis, Writing – review & editing. **Bénédicte Vertruyen:** Conceptualization, Formal analysis, Writing – review & editing. **Abdelfattah Mahmoud:** Conceptualization, Funding acquisition, Formal analysis, Supervision, Writing – review & editing.

Published in : Journal of Power Sources (2023), vol. 55, 232410
DOI: doi:10.1016/j.jpowsour.2022.232410
Status : Postprint (Author's version)

Declaration of competing interest

The authors declare that they have no known competing financial interests or personal relationships that could have appeared to influence the work reported in this paper.

Data availability

The data that has been used is confidential.

Acknowledgments

The authors are grateful to University of Liège and FRS-FNRS for equipment grants. The authors are grateful to the Walloon region for the support under "PE PlanMarshall2.vert" program (BATWAL – 1318146). N.E. thanks FNRS for the PhD FRIA grant [Grant 1.E118.16].

Appendix A. Supplementary data

Supplementary data to this article can be found online at https://doi.org/10.1016/j.jpowsour.2022.232410.

References

[1] B. Dunn, H. Kamath, J.-M. Tarascon, Electrical energy storage for the grid: a battery of choices, Science 334 (2011) 928–935, https://doi.org/10.1126/ science.1212741.

[2] N. Yabuuchi, K. Kubota, M. Dahbi, S. Komaba, Research development on sodium-ion batteries, Chem. Rev. 114 (2014) 11636–11682, https://doi.org/10.1021/ cr500192f.

[3] K. Kubota, M. Dahbi, T. Hosaka, S. Kumakura, S. Komaba, Towards K-ion and Na-ion batteries as "beyond Li-ion", Chem. Rec. 18 (2018) 459–479, https://doi.org/ 10.1002/tcr.201700057.

[4] H. Kim, J.C. Kim, M. Bianchini, D.H. Seo, J. Rodriguez-Garcia, G. Ceder, Recent progress and perspective in electrode materials for K-ion batteries, Adv. Energy Mater. 8 (2018) 1–19, https://doi.org/10.1002/aenm.201702384.

[5] X. Wu, D.P. Leonard, X. Ji, Emerging non-aqueous potassium-ion batteries: challenges and opportunities, Chem. Mater. 29 (2017) 5031–5042, https://doi.org/10.1021/acs.chemmater.7b01764.

[6] S. Komaba, T. Hasegawa, M. Dahbi, K. Kubota, Potassium intercalation into graphite to realize high-voltage/high-power potassium-ion batteries and potassium-ion capacitors, Electrochem. Commun. 60 (2015) 172–175, https://doi. org/10.1016/j.elecom.2015.09.002.

Published in : Journal of Power Sources (2023), vol. 55, 232410
DOI: doi:10.1016/j.jpowsour.2022.232410
Status : Postprint (Author's version)

[7] K. Zaghib, J. Trottier, P. Hovington, F. Brochu, A. Guerfi, A. Mauger, C.M. Julien, Characterization of Na-based phosphate as electrode materials for electrochemical cells, J. Power Sources 196 (2011) 9612–9617, https://doi.org/10.1016/j. jpowsour.2011.06.061.

[8] N. Recham, G. Rousse, M.T. Sougrati, J.N. Chotard, C. Frayret, S. Mariyappan, B. C. Melot, J.C. Jumas, J.M. Tarascon, Preparation and characterization of a stable FeSO4F-based framework for alkali ion insertion electrodes, Chem. Mater. 24 (2012) 4363–4370, https://doi.org/10.1021/cm302428w.

[9] B.L. Ellis, W.R.M. Makahnouk, Y. Makimura, K. Toghill, L.F. Nazar, A multifunctional 3.5V iron-based phosphate cathode for rechargeable batteries, Nat. Mater. 6 (2007) 749–753, https://doi.org/10.1038/nmat2007.

[10] Y. Kawabe, N. Yabuuchi, M. Kajiyama, N. Fukuhara, T. Inamasu, R. Okuyama, I. Nakai, S. Komaba, Synthesis and electrode performance of carbon coated Na_2FePO_4F for rechargeable Na batteries, Electrochem. Commun. 13 (2011) 1225–1228, https://doi.org/10.1016/j.elecom.2011.08.038.

[11] H. Hu, Y. Bai, C. Miao, Z. Luo, X. Wang, Polyfurfuryl alcohol assisted synthesis of Na_2FePO_4F/C nanocomposites as cathode material of sodium ion batteries, J. Electroanal. Chem. 867 (2020), 114187, https://doi.org/10.1016/j. jelechem.2020.114187.

[12] Y. Kawabe, N. Yabuuchi, M. Kajiyama, N. Fukuhara, T. Inamasu, R. Okuyama, I. Nakai, S. Komaba, A comparison of crystal structures and electrode performance between Na_2FePO_4F and $Na_2Fe_{0.5}Mn_{0.5}PO_4F$ synthesized by solid-state method for rechargeable Na-ion batteries, Electrochemistry 80 (2012) 80–84, https://doi.org/ 10.5796/electrochemistry.80.80.

[13] J.S. Ko, V.V.T. Doan-Nguyen, H.S. Kim, X. Petrissans, R.H. Deblock, C.S. Choi, J. W. Long, B.S. Dunn, High-rate capability of Na_2FePO_4F nanoparticles by enhancing surface carbon functionality for Na-ion batteries, J. Mater. Chem. 5 (2017) 18707–18715, https://doi.org/10.1039/c7ta05680j.

[14] W. Ko, J.K. Yoo, H. Park, Y. Lee, H. Kim, Y. Oh, S.T. Myung, J. Kim, Development of Na_2FePO_4F/Conducting-Polymer composite as an exceptionally high performance cathode material for Na-ion batteries, J. Power Sources 432 (2019) 1–7, https://doi.org/10.1016/j.jpowsour.2019.05.066.

[15] H. Li, T. Wang, X. Wang, G. Li, J. Shen, J. Chai, MOF-derived Al-doped Na_2FePO_4F/mesoporous carbon nanonetwork composites as high-performance cathode material for sodium-ion batteries, Electrochim. Acta 373 (2021), 137905, https://doi.org/10.1016/j.electacta.2021.137905.

[16] J. Zhang, X. Zhou, Y. Wang, J. Qian, F. Zhong, X. Feng, W. Chen, X. Ai, H. Yang, Y. Cao, Highly electrochemically-reversible mesoporous Na_2FePO_4F/C as cathode material for high-performance sodium-ion batteries, Small 15 (2019) 1–7, https:// doi.org/10.1002/smll.201903723.

[17] X. Deng, W. Shi, J. Sunarso, M. Liu, Z. Shao, A green route to a Na_2FePO_4F-based cathode for sodium ion batteries of high rate and long cycling life, ACS Appl. Mater. Interfaces 9 (2017) 16280–16287, https://doi.org/10.1021/ acsami.7b03933.

Published in : Journal of Power Sources (2023), vol. 55, 232410
DOI: doi:10.1016/j.jpowsour.2022.232410
Status : Postprint (Author's version)

[18] R. Ling, S. Cai, S. Shen, X. Hu, D. Xie, F. Zhang, X. Sun, N. Yu, F. Wang, Synthesis of carbon coated Na_2FePO_4F as cathode materials for high-performance sodium ion batteries, J. Alloys Compd. 704 (2017) 631–640, https://doi.org/10.1016/j. jallcom.2017.02.075.

[19] J. Xun, Y. Zhang, B. Zhang, H. Xu, L. Xu, Facile synthesis of high electrochemical performance Na_2FePO_4F@CNT&GN cathode material as sodium ion batteries, ACS Appl. Energy Mater. 3 (2020) 6232–6239, https://doi.org/10.1021/ acsaem.0c00323.

[20] R. Ling, S. Cai, D. Xie, W. Shen, X. Hu, Y. Li, S. Hua, Y. Jiang, X. Sun, Double-shelled hollow Na_2FePO_4F/C spheres cathode for high-performance sodium-ion batteries, J. Mater. Sci. 53 (2018) 2735–2747, https://doi.org/10.1007/s10853- 017-1738-6.

[21] M.A. Kirsanova, A.S. Akmaev, D.A. Aksyonov, S.v. Ryazantsev, V.A. Nikitina, D. S. Filimonov, M. Avdeev, A.M. Abakumov, Monoclinic α-Na_2FePO_4F with strong antisite disorder and enhanced Na+ diffusion, Inorg. Chem. 59 (2020) 16225–16237, https://doi.org/10.1021/acs.inorgchem.0c01961.

[22] L. Sharma, P.K. Nayak, E. De La Llave, H. Chen, S. Adams, D. Aurbach, P. Barpanda, Electrochemical and diffusional investigation of Na_2FePO_4F fluorophosphate sodium insertion material obtained from FeIII precursor, ACS Appl. Mater. Interfaces 9 (2017) 34961–34969, https://doi.org/10.1021/ acsami.7b10637.

[23] H. Li, T. Wang, X. Wang, G. Li, J. Shen, J. Chai, Na2FePO4F/Biocarbon nanocomposite hollow microspheres derived from biological cell template as high-performance cathode material for sodium-ion batteries, Chem. Eur J. 27 (2021) 9022–9030, https://doi.org/10.1002/chem.202100096.

[24] L. Sharma, A. Bhatia, L. Assaud, S. Franger, P. Barpanda, Ultra-rapid combustion synthesis of Na_2FePO_4F fluorophosphate host for Li-ion and Na-ion insertion, Ionics 24 (2018) 2187–2192, https://doi.org/10.1007/s11581-017-2376-3.

[25] S. Hua, S. Cai, R. Ling, Y. Li, Y. Jiang, D. Xie, S. Jiang, Y. Lin, K. Shen, Synthesis of porous sponge-like Na_2FePO_4F/C as high-rate and long cycle-life cathode material for sodium ion batteries, Inorg. Chem. Commun. 95 (2018) 90–94, https://doi.org/ 10.1016/j.inoche.2018.07.011.

[26] M. Law, V. Ramar, P. Balaya, Synthesis, characterisation and enhanced electrochemical performance of nanostructured Na_2FePO_4F for sodium batteries, RSC Adv. 5 (2015) 50155–50164, https://doi.org/10.1039/c5ra07583a.

[27] F. Wang, N. Zhang, X. Zhao, L. Wang, J. Zhang, T. Wang, F. Liu, Y. Liu, L.Z. Fan, Realizing a high-performance Na-storage cathode by tailoring ultrasmall Na_2FePO_4F nanoparticles with facilitated reaction kinetics, Adv. Sci. 6 (2019), https://doi.org/10.1002/advs.201900649.

[28] A. Langrock, Y. Xu, Y. Liu, S. Ehrman, A. Manivannan, C. Wang, Carbon coated hollow Na_2FePO_4F spheres for Na-ion battery cathodes, J. Power Sources 223 (2013) 62–67, https://doi.org/10.1016/j.jpowsour.2012.09.059.

[29] M. Brisbois, N. Krins, R.P. Hermann, A. Schrijnemakers, R. Cloots, B. Vertruyen, F. Boschini, Spray-drying synthesis of Na_2FePO_4F/carbon powders for lithium-ion batteries, Mater. Lett. 130 (2014) 263–266, https://doi.org/10.1016/j. matlet.2014.05.121.

Published in : Journal of Power Sources (2023), vol. 55, 232410
DOI: doi:10.1016/j.jpowsour.2022.232410
Status : Postprint (Author's version)

[30] M. Brisbois, S. Caes, M.T. Sougrati, B. Vertruyen, A. Schrijnemakers, R. Cloots, N. Eshraghi, R.P. Hermann, A. Mahmoud, F. Boschini, Na_2FePO_4F/multi-walled carbon nanotubes for lithium-ion batteries: operando Mössbauer study of spray-dried composites, Sol. Energy Mater. Sol. Cell. 148 (2016) 67–72, https://doi.org/ 10.1016/j.solmat.2015.09.005.

[31] A. Mahmoud, S. Caes, M. Brisbois, R.P. Hermann, L. Berardo, A. Schrijnemakers, C. Malherbe, G. Eppe, R. Cloots, B. Vertruyen, F. Boschini, Spray-drying as a tool to disperse conductive carbon inside Na_2FePO_4F particles by addition of carbon black or carbon nanotubes to the precursor solution, J. Solid State Electrochem. 22 (2018) 103–112, https://doi.org/10.1007/s10008-017-3717-x.

[32] A. Mahmoud, S. Caes, M. Brisbois, R.P. Hermann, L. Berardo, A. Schrijnemakers, C. Malherbe, G. Eppe, R. Cloots, B. Vertruyen, F. Boschini, Spray-drying as a tool to disperse conductive carbon inside Na_2FePO_4F particles by addition of carbon black or carbon nanotubes to the precursor solution, J. Solid State Electrochem. 22 (2017) 103–112, https://doi.org/10.1007/s10008-017-3717-x.

[33] N. Eshraghi, S. Caes, A. Mahmoud, R. Cloots, B. Vertruyen, F. Boschini, Sodium vanadium (III) fluorophosphate/carbon nanotubes composite (NVPF/CNT) prepared by spray-drying: good electrochemical performance thanks to well-dispersed CNT network within NVPF particles, Electrochim. Acta 228 (2017) 319–324, https://doi.org/10.1016/j.electacta.2017.01.026.

[34] J. Bodart, N. Eshraghi, T. Carabin, B. Vertruyen, R. Cloots, F. Boschini, A. Mahmoud, Spray-dried K3V(PO4)2/C composites as novel cathode materials for (2020) 480, https://doi.org/10.1016/j.jpowsour.2020.229057.

[35] I.K. Lee, I.B. Shim, C.S. Kim, Phase transition studies of sodium deintercalated Na_2- $xFePO_4F$ ($0 \leq x \leq 1$) by Mössbauer spectroscopy, J. Appl. Phys. 109 (2011) 2009–2012, https://doi.org/10.1063/1.3561798.

[36] X. Lin, J. Huang, H. Tan, J. Huang, B. Zhang, $K_3V_2(PO_4)_2F_3$ as a robust cathode for potassium-ion batteries, Energy Storage Mater. 16 (2019) 97–101, https://doi.org/ 10.1016/j.ensm.2018.04.026.

[37] S. Bublil, M. Fayena-Greenstein, M. Talyanker, N. Solomatin, M.N. Tsubery, T. Bendikov, T.R. Penki, J. Grinblat, I.B. Dur´an, I. Grinberg, Y. Ein-Eli, Y. Elias, P. Hartmann, D. Aurbach, Na-ion battery cathode materials prepared by electrochemical ion exchange from alumina-coated $Li_{1+x}Mn_{0.54}Co_{0.13}Ni_{0.1+y}O_2$, J. Mater. Chem. 6 (2018) 14816–14827, https://doi.org/10.1039/c8ta05068f.

[38] Y. Zhang, H. Yu, H. Zhou, Two-electron migration orthosilicate cathode materials for Na-ion batteries, J. Mater. Chem. 2 (2014) 11574–11577, https://doi.org/ 10.1039/c4ta01819b.

[39] S.M. Oh, S.T. Myung, J. Hassoun, B. Scrosati, Y.K. Sun, Reversible Na_2FePO_4F electrode for sodium secondary batteries, Electrochem. Commun. 22 (2012) 149–152, https://doi.org/10.1016/j.elecom.2012.06.014.

[40] H. Liu, J. Xu, C. Ma, Y.S. Meng, A new O3-type layered oxide cathode with high energy/power density for rechargeable Na batteries, Chem. Commun. 51 (2015) 4693–4696, https://doi.org/10.1039/c4cc09760b.

Published in : Journal of Power Sources (2023), vol. 55, 232410
DOI: doi:10.1016/j.jpowsour.2022.232410
Status : Postprint (Author's version)

[41] C. Zhu, C. Wu, C. Chen, P. Kopold, P.A. Van Aken, J. Maier, A high power - high energy $Na_3V_2(PO_4)_2F_3$ sodium cathode: investigation of transport parameters, rational design and realization, Chem. Mater. 29 (2017) 5207–5215, https://doi. org/10.1021/acs.chemmater.7b00927.

[42] K. Wang, R. Cai, T. Yuan, X. Yu, R. Ran, Z. Shao, Process investigation, electrochemical characterization and optimization of $LiFePO_4$/C composite from mechanical activation using sucrose as carbon source, Electrochim. Acta 54 (2009) 2861–2868, https://doi.org/10.1016/j.electacta.2008.11.012.

[43] W.L. Liu, J.P. Tu, Y.Q. Qiao, J.P. Zhou, S.J. Shi, X.L. Wang, C.D. Gu, Optimized performances of core-shell structured $LiFePO_4$/C nanocomposite, J. Power Sources 196 (2011) 7728–7735, https://doi.org/10.1016/j.jpowsour.2011.05.046.

[44] J. Dong, J. Xiao, Y. Yu, J. Wang, F. Chen, S. Wang, L. Zhang, N. Ren, B. Pan, C. Chen, Electronic structure regulation of Na_2FePO_4F cathode toward superior high-rate and high-temperature sodium-ion batteries, Energy Storage Mater. 45 (2022) 851–860, https://doi.org/10.1016/j.ensm.2021.12.034.